Experimental determination of Ni isotope fractionation during Ni adsorption from an aqueous fluid onto calcite surfaces

Cristina Castillo Alvarez, Ghylaine Quitté, Jacques Schott, Eric H Oelkers

EXPERIMENTAL DETERMINATION OF Ni ISOTOPE FRACTIONATION DURING Ni ADSORPTION FROM AN AQUEOUS FLUID ONTO CALCITE SURFACES

Cristina Castillo Alvarez [a], Ghylaine Quitté [b], Jacques Schott [a] and Eric H. Oelkers [a,c]

[a] GET, CNRS-Université de Toulouse, UMR 5563, 31400 Toulouse, France, [b] IRAP, Université de Toulouse, CNRS, UPS, CNES, UMR 5277, 31400 Toulouse, France, [c]London Geochemistry and Isotope Centre (LOGIC), University College London and Birkbeck, University of London, Gower Place, London, UK.

Abstract

The fractionation of Ni isotopes during Ni adsorption from aqueous fluids onto calcite surfaces was measured at 25 ^{o}C and as a function of pH from 7.7 to 8.9. Experiments showed that the percent Ni adsorbed and the degree of Ni isotope fractionation attained constant values in less than 30 hours after the calcite was exposed to the Ni bearing, calcite saturated aqueous solution. The percentage of Ni adsorbed from the fluid onto the calcite surfaces increased from 9 to 67% as the pH increased over this range. Calcite preferentially adsorbs light Ni isotopes during adsorption, resulting in a fractionation between adsorbed and aqueous, $\Delta^{60}Ni_{calcite\text{-}fluid}$, of -0.52±0.16‰. This value is pH independent, within uncertainty, over the experimental pH range. The preferential adsorption of light Ni isotopes into calcite likely results from the change in coordination environment between adsorbed and aqueous nickel; the Ni-O length in the Ni-CO_3 bond formed at the calcite surface is greater than that in the Ni^{2+} aquo ion.

1. INTRODUCTION

The interpretation of the Ni isotope compositions in the marine record is facilitated by a detailed understanding of the mechanisms and extent of Ni isotope fractionation during natural fluid-mineral processes. Towards this goal, equilibrium isotopic fractionation between Ni adsorbed onto calcite surfaces and its coexisting aqueous fluids was measured as a function of pH

at 25 ^{o}C. The purpose of this paper is to report the results of this experimental study and to use these results to better understand the isotopic fractionation of Ni during its interaction with mineral surfaces.

The quantification of isotopic fractionation among fluids and major minerals help constrain the size and importance of element sources and sinks on a global scale. For example, the global marine Ni budget is controlled by the input of dissolved Ni from river water, dissolution in the oceans of riverine and atmospheric transported particulate material, Ni scavenging by sinking marine mineral particles, and geothermal activity (Ciscato et al., 2018; Jeandel and Oelkers, 2015; Sclater et al., 1976). Based on isotopic compositions of these sources and sinks, several studies concluded that another source of heavy Ni or another sink of light Ni is needed to account for the Ni isotope composition of the global oceans (Cameron and Vance, 2014; Gall et al., 2013; Gueguen et al., 2013; Porter et al., 2014). A number of processes have been suggested as the possible light Ni sink, including the adsorption of Ni onto Fe and/or Mn oxide surfaces (Peacock and Sherman, 2007). The role of such surfaces is underscored by the release of Ni from Mn oxides as the age and transform in marine sediments (Atkins et al., 2014, 2016). Experimental work by Wasylenki et al. (2015) shows that Ni sorption onto ferrihydrite surfaces favors the incorporation of light Ni, leaving an isotopically a heavier aqueous Ni behind. Gall et al. (2013), based on the analysis of the Ni isotope compositions of modern marine precipitated ferrihydrite, concluded that the drawdown of light Ni by its sorption to ferrihydrite was, however, of insufficient magnitude to balance the marine Ni cycle. An alternative sink to potentially resolve this imbalance is the uptake of Ni by sulfides associated with anoxic or suboxic marine sediments enriched in organic matter (Eiler et al., 2014; Gueguen et al., 2013). The present study is the first of two manuscripts that evaluates the role of nickel-calcite interaction during natural processes. This manuscript reports on the experimental measurement of Ni isotope fractionation as it adsorbs ion calcite surfaces. A follow-up study will report experimental measurement of Ni isotope fractionation during its co-precipitation with calcite. Taken together, these studies will help illuminate the potential role of nickel-calcite interaction on the global marine Ni isotope budget.

Nickel isotope fractionation has received attention due to its potential use as a tracer of biochemical processes (Cameron et al., 2009). Nickel exhibits a nutrient-like behavior, with its dissolved concentration ranging from 2 nmol/kg at the ocean surface to 12 nmol/kg at greater

depths (Sohrin and Bruland, 2011). Interest in Ni isotope fractionation as a tracer of organic processes stems in part from results of ab-initio calculations performed by Fujii et al. (2011), who reported that aqueous Ni-organic complexes exhibit a unique Ni isotope fractionation behavior. Indeed, laboratory experiments documented significant Ni isotope fractionation during its incorporation into methanogens (Cameron et al., 2009) and uptake by plants (Estrade et al., 2015).

Nickel adsorption onto calcite surfaces is also of interest due to its unique adsorption behavior. Ni adsorbs on calcite by rearranging the solid surface through the formation of Ni-carbonate surface complexes (Hoffmann and Stipp, 2001; Stipp et al., 1994). These surface complexes are partly hydrated and readily exchangeable due to the high hydration energy of Ni (Zachara et al., 1991). Nevertheless, hydrated Ni complexes on calcite surfaces are more stable than those of other divalent metal complexes (Hoffmann and Stipp, 2001). The degree to which these unique Ni adsorption properties affect its isotopic fractionation will be evaluated with the aid of this experimental study.

2. MATERIALS AND METHODS

2.1 Experimental design

Experiments were performed to determine the equilibrium Ni stable isotope fractionation between aqueous Ni and Ni adsorbed on the calcite surface. Three series of experiments were conducted. First, Ni was adsorbed onto calcite surfaces at constant pH and aqueous Ni concentration as a function of time to evaluate the kinetics of this reaction. Second, Ni was adsorbed onto calcite surfaces at constant pH and various aqueous Ni concentrations. Third, Ni was adsorbed onto calcite surfaces at constant aqueous Ni concentrations and various pH. In all cases, the concentration of Ni in the aqueous solution was kept below the solubility of gaspeite ($NiCO_3$, c.f. Lakshtanov and Stipp, 2007) to avoid its precipitation during the experiments. Each experimental series consisted of a set of individual batch experiment, so that the fluid and solid could be collected and analyzed at each experimental condition.

Synthetic high purity Merck MESURE® calcite was used for all experiments. Prior to its use in the experiments, this calcite was first washed in distilled acetone, then pretreated according to the method described by Reddy and Nancollas (1971). The purity of the resulting calcite

powder was assessed by X-ray diffraction using an INEL CPS-120 diffractometer with Co Kα-radiation having a detection limit of ~5%. The acquired diffraction patterns were compared to the characteristic profile for calcite taken from the RRUFF database (Lafuente et al., 2016). This comparison confirmed the solid to be pure calcite. The surface area of the resulting calcite was 0.31±0.03 m^2/g as determined by triple-point krypton adsorption according to the BET method (Brunauer et al., 1938), using a Quantachrome Autosorb-1MP instrument. Scanning Electron Microscope (SEM) images of this initial calcite were obtained using a JEOL JSM 6700F spectrometer at the Raimond Castaing Center for micro-characterization in Toulouse, France. Resulting images are displayed in Fig. 1. They show the rhombohedral morphology of the calcite crystals, as well as intergrowth and agglomeration. These SEM images were also used to determine the average length of the calcite crystal to be about 6µm.

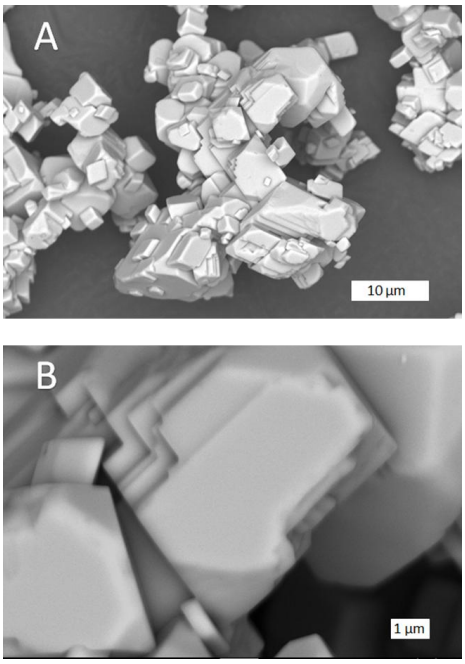

Figure 1. SEM images of the synthetic calcite used in the present study. The scale bar in image A is 10 µm long, whereas the scale bar in image B is 1 µm long.

The initial aqueous fluids used in the experiments were pre-equilibrated with the same calcite used in the experiments. These pre-equilibrated fluids were prepared by adding approximately 2 g of calcite to an aqueous solution having a total ionic strength of 0.01 mol/kg. The initial fluids were prepared by adding reagent grade NaCl, HCl and/or NaOH to 18.2 MΩ water obtained from a Millipore system. The pH of the aqueous solutions was then adjusted to a value from 7.6 to 8.8 for the pH dependent experiments, or to 8.3 for the time dependent and

adsorption isotherm experiments by adding either HCl or NaOH. This fluid remained in contact with the calcite for up to 3 weeks until the measured pH was constant. The pre-equilibrated fluids were separated from the calcite by filtration using a Merck Millipore 0.22 µm teflon syringe filter prior to its use. The aqueous Ni stock solutions added to these fluids for subsequent adsorption experiments were created by dissolving Sigma-Aldrich, 99.99 %, trace metal basis $Ni(NO_3)_2$ to 18.2 M**Ω** water to obtain a total Ni concentration of 6 ppm Ni.

All adsorption experiments were performed in 50 mL screw top polycarbonate centrifuge tubes. The polycarbonate tube reactors were cleaned before their use with 1 M double distilled HCl for 24 hrs, then rinsed several times with 18.2 M**Ω** H_2O, and air dried. Before starting the Ni sorption experiments, several tests were conducted to ensure that no nickel was adsorbed on the walls of the polycarbonate tubes from aqueous solutions at the pHs investigated in this study. These tests consisted of adding aqueous solutions containing 100ppb Ni to the reactors at various pH. No measurable loss of Ni from the starting solution was observed after a period of 1 day during which the reactor tubes were continuously shaken. It was thus assumed that all Ni lost from solution during the experiments was due to its adsorption onto calcite surfaces.

Each experiment was initiated by placing a known quantity of calcite powder and 30 mL of a Ni-free aqueous solution pre-equilibrated with calcite into the tube reactor. Each reactor was closed and mixed on a rotator for 24 hours. After this time a selected quantity of the aqueous Ni stock solution was added to the initial calcite-aqueous fluid mixture, prior to reclosing the tube. This mixture was then returned to the rotator. Several additional experiments were run in the absence of added Ni to verify no nickel was released to solution from the calcite present in the reactor. After a given time period (72 hours for the pH dependent experiments, from 0.5 to 168 hrs for the time dependent series, and 24 hrs for the Ni adsorption isotherm), a reactor tube was removed from the rotator and the reactor tube with its content was centrifuged for 15 minutes at 4500 rpm on an Eppendorf 5804 centrifuge. The reactor tube was then opened and the solids were separated from the fluid phase using a 0.2 micron Teflon Merck Millipore filter. A minimum of 28.5 mL of fluid was recovered from each reactor. The collected fluids were separated into three subsamples: one of the subsamples was used to measure pH immediately after sampling, while the other two samples were acidified, one with ultrapure HNO_3 and the other with ultrapure HCl for Ni elemental and isotopic analyses, respectively.

2.2 Chemical analyses

Nickel concentrations of the initial stock solutions and collected fluid samples of each experiment were determined using an Atomic Absorption Spectrometer Perkin Elmer AAnalyst 600 together with a graphite furnace. Concentrations were obtained from measured absorbance using a calibration curve generated from standards having concentrations ranging from 10-100 ppb. New standards were prepared and new calibration curves were made each day the analyses were performed. A 0.05M NH_4Cl matrix modifier was used during the measurements. The uncertainties on these analyses, based upon duplicated measurements are estimated to be ± 2% whereas the detection limit was 1.5ppb.

The pH of fluid samples was measured immediately after sampling using a standard Mettler Toledo glass pH electrode. This electrode was calibrated before every measurement using Thermo Fisher pH=4.006, 6.865 and 9.183 buffer solutions at 25°C. The uncertainties on these pH measurements are estimated to be ±0.03 pH units.

2.3 Ni isotope analysis

2.3.1 Isotopic notation

Isotopic compositions in this paper are presented in delta notation, δ^{60}Ni, corresponding to the ratio of ^{60}Ni relative to ^{58}Ni normalized to the Sigma Aldrich ICP standard. This standard was used rather than the certified SRM986 standard as what is essential to this study of fractionation during adsorption is the change in δ^{60}Ni during experiments rather than its absolute value. The difference in the Ni isotope composition the solid and the fluid phase ($\Delta\ ^{60}\mathrm{Ni}_{solid-fluid}$) is defined by

$$\Delta\ ^{60}\mathrm{Ni}_{solid-fluid} = \delta^{60}\mathrm{Ni}_{solid} - \delta^{60}\mathrm{Ni}_{fluid} \quad (1)$$

All isotopic measurements reported in this study were performed on the aqueous solutions after filtration. These values used to determine the isotopic composition of the solids because 1) the much higher sensitivity of solutions to the minor changes in isotopic composition compared to the bulk solid, 2) the possibility that some Ni was present in the original calcite grains, 3) the

potential for some Ni to desorb from calcite surfaces after sampling, and 4) the possibility that some Ni from the fluid phase would precipitate onto the calcite surfaces as they were dried. Indeed several analyses of the solids recovered from the experiments showed their Ni isotope compositions to be highly scattered and inconsistent. Because the reacting solution was undersaturated with respect to $NiCO_3$ (gaspeite) and Ni adsorption on the reactor walls was insignificant, it can be assumed that the loss of Ni from the aqueous solution was solely caused by Ni sorption on calcite. The average isotopic composition of adsorbed Ni onto calcite during a closed system adsorption experiment can thus be calculated from the initial and final Ni chemical and isotopic compositions of the fluid and mass balance considerations taking account of (Criss, 1999)

$$\delta^{60}\mathrm{Ni}_{total} m_{\mathrm{Ni},total} = \delta^{60}\mathrm{Ni}_{solid} m_{\mathrm{Ni},solid} + \delta^{60}\mathrm{Ni}_{fluid} m_{\mathrm{Ni},fluid} \qquad (2)$$

where $m_{\mathrm{Ni},solid}$ and $m_{\mathrm{Ni},fluid}$ refer to the mass of Ni adsorbed onto the calcite surface and present in the aqueous fluid phase, respectively. Note that $\delta^{60}\mathrm{Ni}_{total}$ and $m_{\mathrm{Ni},total}$ are constant during a closed system reactor experiment. A similar approach to calculate the isotopic composition of adsorbed elements was used for Mo (Barling and Anbar, 2004), B (Lemarchand et al., 2005, Lemarchand et al., 2007), Cu and Zn (Balistrieri et al., 2008), Si (Delstanche et al., 2009, Oelze et al., 2014), and Ge (Pokrovsky et al., 2014). Equations (1) and (2) are used below to calculate the isotopic composition of Ni adsorbed to calcite surfaces from corresponding fluid isotope compositions.

2.3.2 Sample purification

Prior to the measurement of Ni isotope ratios by mass spectrometry, Ni was separated using an approach based on Quitté and Oberli (2006). This separation procedure was performed under a laminar flow hood using trace metal grade NH_4OH and H_2O_2, and doubly distilled HNO_3 and HCl. The overall purification of the samples consisted of five separation steps:

1) Step one began by evaporating the sample to dryness in Savillex Teflon containers. The resulting residue was dissolved in 2 mL of 9 M aqueous HCl. An ion exchange column was prepared by adding 1.8 mL of pre-cleaned, Bio-Rad 100–200 mesh AG1-X8 anion resin to a 10-mL polypropylene column. The resin was cleaned with alternating 6M HCl

and 18.2 MΩ H_2O and then conditioned by passing 10 mL of 9M HCl through the column. The 2 mL sample was then passed through the column to remove Fe from the sample. Nickel eluted immediately. A further 4 mL of 9M HCl was added to the column to ensure the complete recovery of Ni.

2) Step two aimed to remove Zn from the sample. It began by evaporating the Ni collected from the first step to dryness and re-dissolving it into 2 mL of 2 M HCl. This sample was passed through the same ion exchange column as in the first step described above but conditioned this time by passing 10 mL of a 2M HCl through the column. The sample was loaded on the column in 2mL 2M HCl, once again Ni eluted immediately, and a further 4 mL of 2M HCl was passed through the column to ensure the complete recovery of Ni.

3) Step three separated the major matrix elements from the sample. It began by evaporating the Ni elution sample collected from step 2 to dryness then redissolving it into 5 mL of 1 M HCl and 1 mL of 1M ammonium citrate solution. The ammonium citrate solution was prepared by mixing a citric acid solution and a trace grade NH_4OH solution. Once the pH of the redissolved Ni bearing solution was adjusted to 8-9 using NH_4OH, the sample was loaded onto a column filled with 2 mL of Triskem Nickel specific resin (based on dimethylglyoxime, DMG). Prior to its use, this resin was cleaned with water and ammonium citrate and conditioned with 5 mL of 0.2M of ammonium citrate whose pH was adjusted to 8-9 using NH_4OH. After the sample was loaded onto the resin, it was washed with 20 mL of 0.2 M ammonium citrate (adjusted to pH=8-9) to remove matrix elements. Nickel was then recovered from the column by passing 12 mL of 3M HNO_3. Three drops of perchloric acid were added to the recovered Ni fraction to destroy the DMG-Ni complex and the sample was evaporated to dryness. The sample was then taken up in 1mL of concentrated HNO_3 and 1mL of ultrapure H_2O_2 and heated for a few hours to remove potential organics and ensure a complete release of Ni from the DMG-Ni complex. The sample was then evaporated again. If necessary, this oxidation procedure was repeated twice. The complete removal of this complex was verified by the white color of the residual solids following the oxidation procedure.

4) Step four is a purification step. The cleaned residue was dissolved into 0.2mL of 18.2 MΩ H_2O and passed through a column containing 0.12 mL of Bio-Rad AG50W-X8 resin

(200–400 mesh), previously cleaned twice with H_2O and 6M HCl, then conditioned with water. The matrix elements were removed with 2.5 mL of 0.2M HCl and then Ni was recovered in 0.5 mL of 3M HCl.

5) The final step removed any remaining Fe from the sample (including Fe released by the resin) following closely the protocol of step 1 or 2, replacing the 9M or 2M HCl by 6M HCl. A summary of these steps is provided in Table 1.

Table 1 Summary of the purification procedure used to prepare fluid samples for Ni isotope analysis by mass spectrometry.

	Reagent	volume (mL)
Col. 1		
Resin	AG1-X8	2
Conditioning	2M HCl	10
Load	2M HCl *	2
Ni elution	2M HCl	4
Col. 2		
Resin	AG1-X8	2
Conditioning	9M HCl	10
Load	9M HCl *	2
Ni elution	9M HCl	4
Col. 3		
Resin	Nickel specific	2
Conditioning	0.2M $(NH_4)_3C_6H_8O_7$	12
Load	1M $(NH_4)_3C_6H_8O_7$ +1M HCl	1+5
clean matrix	0.2M $(NH_4)_3C_6H_8O_7$	20
Ni elution	3M HNO_3	12
Col. 4		
Resin	AG50W-X8	0.15
Conditioning	H_2O	0.7
Load	H_2O	0.2
clean matrix	0.2M HCl	2.5
Ni elution	3M HCl	0.5
Col. 5		
Resin	AG1-X8	2
Conditioning	6M HCl	10
Load	2M HCl *	2
Ni elution	2M HCl	4

* Ni starts eluting during this step

2.3.3 Mass spectrometry

The Ni bearing fluid sample recovered from step 5 of the purification procedure was dried. This residue was dissolved into 0.1M HCl prior to isotopic analysis. Nickel isotope measurements were performed at the Observatiore de Midi Pyrenees analytical platform in Toulouse France, using a Thermo-Finnigan Neptune multi-collector inductively coupled plasma mass spectrometer (MC-ICPMS) equipped with an Apex desolvating system connected to a glass nebulizer, and fitted with a standard sample cone and a X skimmer cone. Samples were measured in medium resolution mode to avoid interferences such as with ArO^{+}. Instrumental mass bias was corrected using sample-standard bracketing techniques and Cu doping; this approach has been regularly validated in our laboratory using the PCC-1 standard yielding an average value of 0.08±0.04‰.amu^{-1}, in excellent agreement with literature data (Gall et al. 2012; Gueguen et al. 2013; Chernonozhkin et al. 2016). The concentration of the measured samples, always adjusted to match those of the standard within 10%, varied between 50 and 200 ppb, and the Cu concentration was half that of Ni. Samples were measured in 2 cycles. During the first cycle, stable Ni isotope masses were measured (58, 60, 61, 62 and 64) along with masses 57 and 66, which are used to correct for possible isobaric interference from ^{58}Fe and ^{64}Zn, respectively. During the second cycle, Cu isotopes were measured together with Ni isotopes and used to correct for instrumental mass bias. In detail, the Cu-doped standard was measured during every other run, each sample interspersed between two standards. The instrumental mass bias was calculated using the exponential law for the Cu isotope ratio in the sample (hence matrix matched) and then applied to the Ni ratios; the Cu-corrected Ni ratios were then normalized to the Cu-corrected average ratio of the two bracketing standards. Typically, a 200ppb Ni solution yielded a total ion beam of 30V. To check for Ni fractionation during the column separation, two tests were performed: (1) first, the Sigma Aldrich standard solution was processed through the whole chemical separation procedure with every set of experimental samples and measured; (2) second, a carbonate sample similar to those used in the experiments, initially devoid of Ni but doped with our Sigma Aldrich Ni standard solution, was processed. Both tests yield a Ni isotope composition indistinguishable from the matrix-free unprocessed standards. Hence, no isotopic fractionation is observed for the processed standards relative to the corresponding unprocessed standards, confirming that the chemical procedure is well suited to quantify the natural mass

dependent isotopic fractionation characteristic of our experimental samples (Figure 2). The 2SD (standard deviations) of δ^{60}Ni was calculated based on multiple (typically 3) measurements of each Ni sample and ranged from 0.01 to 0.19‰.

A double spike approach was not used for Ni isotope analyses in this study to avoid machine contamination; the MC-ICPMS used in this study is also routinely used for the measurement of Ni in cosmochemistry samples, which are particularly sensitive to small uncertainties in ^{61}Ni, ^{62}Ni and ^{64}Ni. The Cu doping method adopted in this study has been shown to have a reproducibility comparable to that attained using a double spike approach (Quitté and Oberli, 2006).

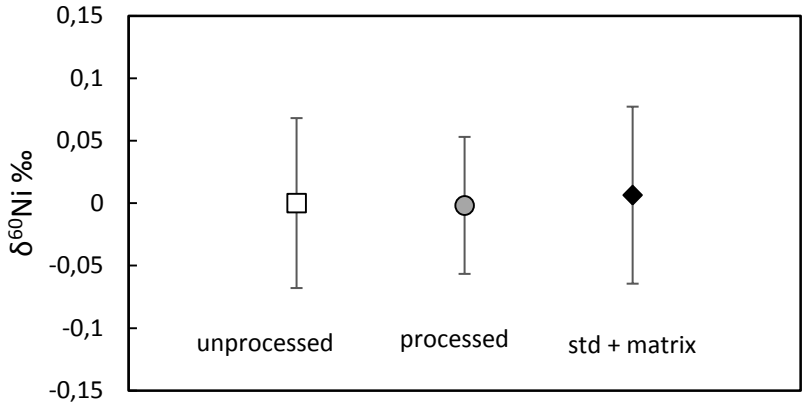

Figure 2. Ni isotope compositions of processed and unprocessed standards used to validate the Ni separation protocol. The open square represents the isotopic composition of the unprocessed standard, the filled circle shows the composition of the processed standard, and the filled diamond shows the composition of a standard diluted to the approximate concentration of the experiments reported in this study (listed as std + matrix).

2.4 Geochemical Calculations

All thermodynamic calculations, including aqueous fluid speciation calculations and mineral solubility calculations, were performed using PHREEQC (Parkhurst and Appelo, 2015) together with its minteq.v4 database.

3. RESULTS

A total of 28 individual batch experiments were performed in the three series. The conditions and measured fluid compositions of these experiments are reported in Tables 2 and 3. The first experimental series, series K, was designed to assess if Ni adsorption onto calcite surfaces and its associated fractionation are time dependent. The results of this series are shown in Figure 3 for reaction times from 3 to 168 hrs. It can be seen that the extent of Ni adsorption increases slightly during the first 24 hrs but remains constant afterwards. In contrast, isotopic steady-state is attained only after ~30 hrs, although the isotopic composition of adsorbed Ni becomes very slightly lighter with time after this, which may reflect some incorporation of Ni into the calcite lattice.

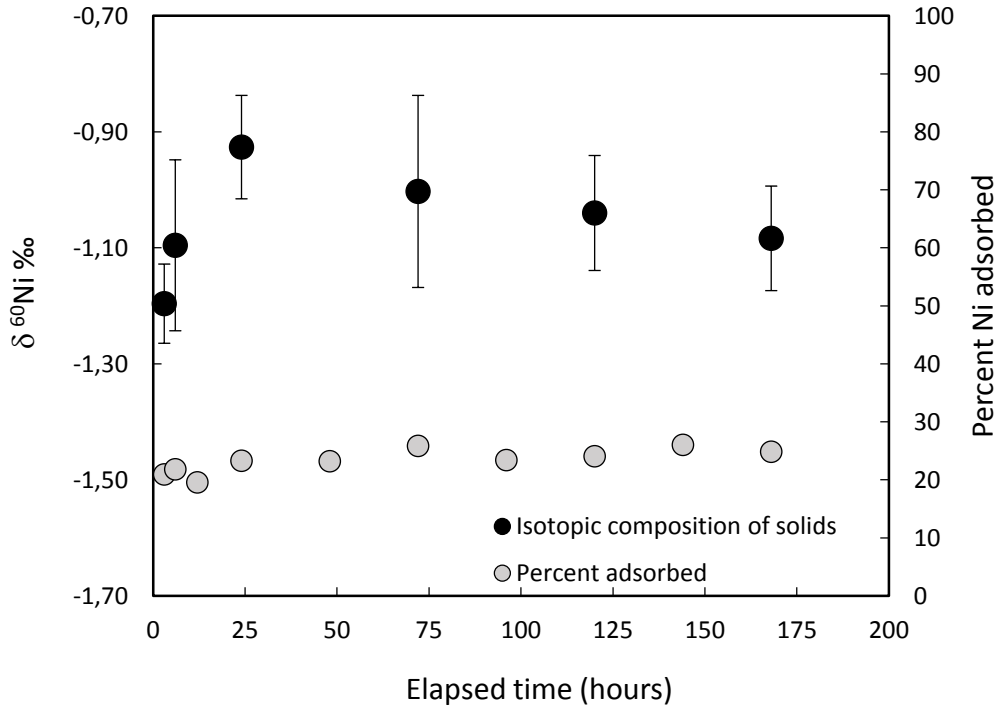

Figure 3. Percent of Ni adsorbed onto calcite surfaces and the Ni isotope composition of this adsorbed Ni as a function of elapsed time at 25 ^{o}C and pH 8.3. The percent Ni adsorbed is shown as grey circles and their values are given in the right hand scale, whereas the corresponding Ni isotope composition of the solids is shown as black circles, these values are given by the left axis. The isotope composition of the solids was obtained from the measured aqueous Ni isotope composition using mass balance considerations. The uncertainties on the measured adsorption percent are approximated by the symbol size. The 2D standard deviations of the Ni isotope compositions shown in this figure are provided in Table 3.

A second experimental series, series I, was designed to assess the partition coefficient of Ni onto calcite surfaces. This series was run at a pH of 8.3 and the aqueous Ni concentrations varied from 60 to 120 ppb. The Ni concentrations in this experimental series were limited on one hand by the analytical detection limits for Ni and on the other hand by the requirement to keep this fluid undersaturated with respect to gaspeite ($NiCO_3$). A linear correlation between the concentration of aqueous Ni and adsorbed Ni was observed (see Fig. 4) consistent with adsorption being the predominant mechanism for Ni loss from solution. The apparent partition coefficient of Ni at pH=8.3 (K_d) was calculated to be

$$K_d = (m_{Ni\text{-}ads}/m_{solid})/(m_{Ni\text{-}aq}/m_{solution}) = 0.011.$$

where m_i refers to the mass of the subscripted species or phase. Note that Ni isotope compositions were not determined for the samples collected from this experimental series.

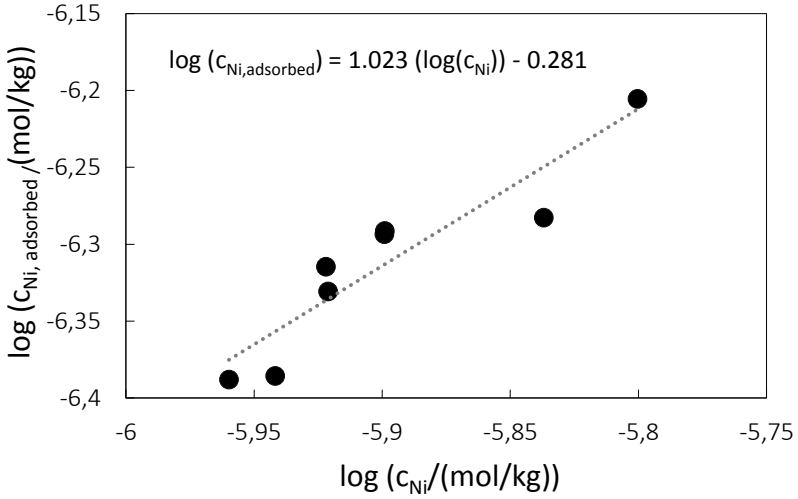

Figure 4 Variation of the Ni concentration adsorbed onto calcite surfaces as a function of the aqueous Ni concentration at 25 ^{o}C. The line shown through the data points corresponds to a least squares fit of the data; the equation of this line is provided on the figure. The uncertainties in these measurements are within the size of the symbols.

Table 2: Measured aqueous and adsorbed Ni concentrations of samples collected from experimental series I, designed to determine partition functions at 25°C and pH 8.3.

Experiment	Aqueous Ni conc. *Mol/kg*	Adsorbed Ni conc. *Mol/kg*
I01	1.10×10^{-6}	4.09×10^{-7}
I02	1.14×10^{-6}	4.11×10^{-7}
I03	1.26×10^{-6}	5.11×10^{-7}
I04	1.46×10^{-6}	5.21×10^{-7}
I05	1.58×10^{-6}	6.23×10^{-7}
I06	1.26×10^{-6}	5.09×10^{-7}
I07	1.20×10^{-6}	4.84×10^{-7}
I08	1.20×10^{-6}	4.67×10^{-7}

A third experimental series, series P, determined the amount of Ni adsorbed onto calcite surfaces as a function of pH from 7.6 to 8.8. The results, shown in Fig. 5, illustrate the increase in the percent of Ni adsorbed from 8.7 to 67 % as the pH increased over this range. The Ni isotope composition of the fluids and solids recovered from this experimental series, as well as those of experimental series P run for the same elapsed time, are plotted as a function of the fraction of Ni adsorbed on calcite in Fig 6a. Note that whereas the Ni isotope compositions of the fluids in this figure were directly determined from measurements, those of the solids were determined from the measured fluid compositions and mass balance constraints (see Eq. 2). The associated uncertainty was determined by error propagation, taking into account the uncertainty on the isotopic composition of the fluid and on the Ni concentrations of the fluid and solid phase. It can be seen that all experiments exhibit a preferential sorption lighter Ni lighter on the calcite surface, leaving the aqueous Ni isotopically heavier than the initial Ni stock solution which had a $\delta^{60}Ni = -0.63 \pm 0.05$‰. The offset between the aqueous fluid and adsorbed Ni compositions is independent of the percentage of Ni adsorbed within uncertainty, which suggests that Ni isotope fractionation during adsorption on calcite surface occurs at equilibrium. The extent of Ni isotope fractionation between the calcite surface and the aqueous fluid is plotted as a function of pH in Figure 6b. It can be seen that the difference in the Ni isotope composition between the solid and solution, $\Delta^{60}Ni_{calcite\text{-}fluid} = -0.52 \pm 0.16$‰, does not vary significantly as the pH increases from 7.7 to 8.6. A slight increase in $\Delta^{60}Ni_{calcite\text{-}fluid}$ (by about 0.04‰) at the lowest Ni surface coverage is suggested

by the data. However, one should note the large uncertainty affecting the data for the lowest extents of Ni sorption (see Fig. 6b).

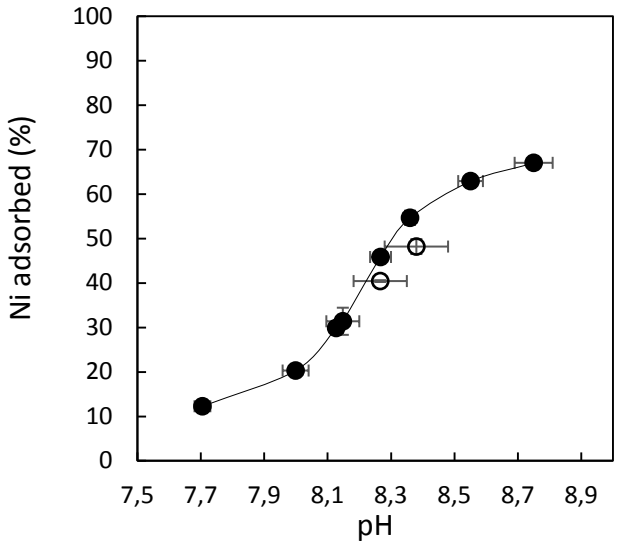

Figure 5. The percent Ni adsorbed from the aqueous solution onto calcite surfaces as a function of pH at 25 ^{o}C. The filled symbols correspond to experiments where the isotopic compositions of Ni were determined, whereas these were not determined for experiments shown as open symbols.

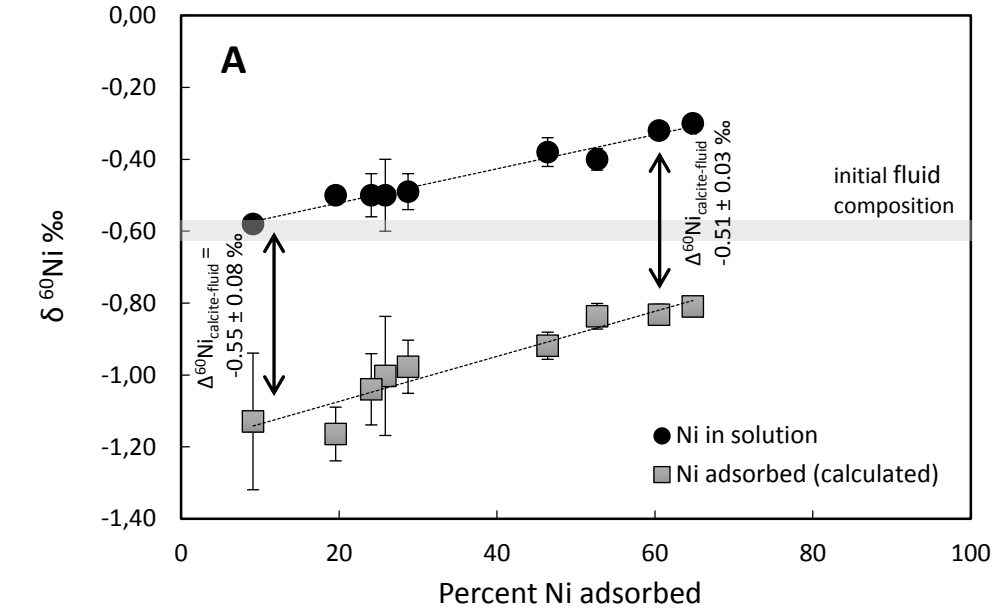

361

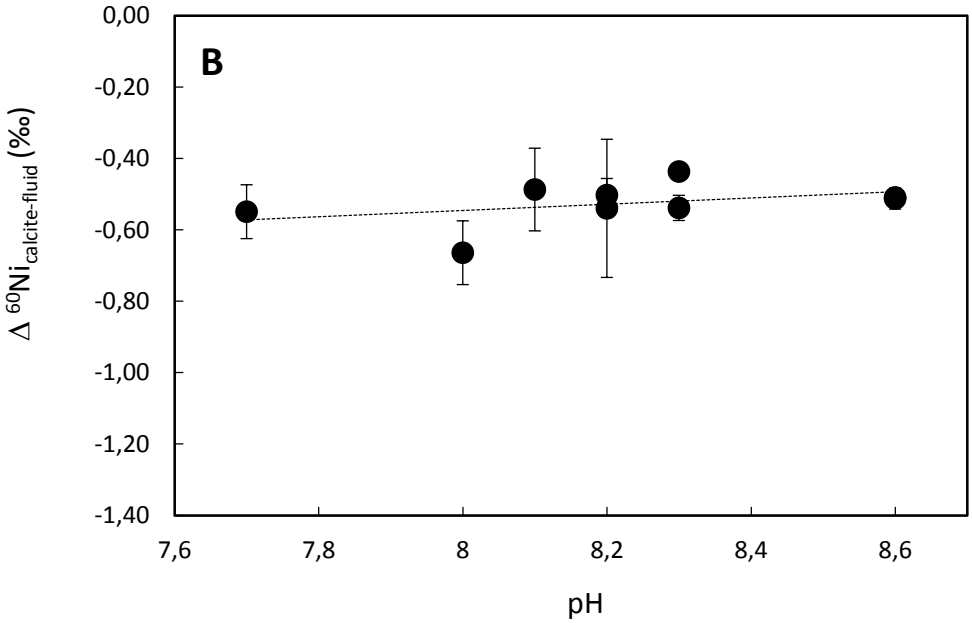

362

363 Figure 6 a) Ni isotope composition of the adsorbed and aqueous Ni as a function of percentage of
364 Ni adsorbed and b) $\Delta^{60}Ni_{calcite\text{-}fluid}$ as a function of pH. In figure 6a, the black circles represent the
365 Ni isotope compositions of the aqueous solutions, which were directly measured. The grey
366 squares represent the isotopic compositions of the Ni adsorbed onto calcite surfaces, which were
367 obtained from mass balance calculations – see text. The gray band shows the initial isotopic
368 composition of the solution, which was -0.63±0.05‰. The dashed lines in these figures represent
369 a least squares fit to the data points.

4. DISCUSSION

4.1 Comparison of Ni adsorption behavior with previous studies.

The nickel sorption isotherm, plotted on a log-log scale in Fig. 4, exhibits a linear trend with a slope close to 1 similar to what has been reported in past studies (Belova et al., 2014; Lakshtanov and Stipp, 2007; Zachara et al., 1991). This behavior indicates that Ni partitioning between solid and liquid phases does not depend on the Ni concentration. The apparent partition coefficient deduced from the data shown in Fig, 4, K_{Ni} = 0.011 at pH = 8.3 is in good agreement with the value extracted from Zachara et al. (1991) at the same pH (K_{Ni} = 0.012). The maximum Ni adsorption in the experiments presented above is attained after only a few hours, which is consistent with previous work on the absorption onto calcite of Ni (Zachara et al., 1991) and other divalent cations (McBride, 1980; Zachara et al., 1988). Our experiments show no variation in the amount of Ni adsorbed on the calcite surface as time progresses; a similar behavior was observed for Ni adsorption on ferrihydrites and goethite (Wasylenki et al. 2015) and Zn on calcite (Dong and Wasylenki, 2016).

Nickel adsorption onto calcite surfaces increases with pH to at least pH ~ 9 which is in agreement with the previous studies (Belova et al., 2014; Tahervand and Jalali, 2017; Zachara et al., 1991). This behavior can be attributed to the buildup of a negative charge on calcite surface. According to calcite surface complexation models (Pokrovsky et al., 2000, 1999; Van Cappellen et al., 1993), Ni adsorption onto calcite can be described according to (Pokrovsky et al., 2002):

$$>CO_3^- + Ni^{2+} = >CO_3Ni^+ \quad (3)$$

where $>CO_3^-$ and $>CO_3Ni^+$ stand for a deprotonated carbonate site and the Ni surface complex formed on this carbonate site, respectively. The increase of $>CO_3^-$ concentration with increasing pH to ~ 9 accounts for the observed corresponding increase of Ni sorption.

4.2 Interpretation of Ni isotope fractionation during its adsorption onto calcite surfaces.

A number of past studies have measured Ni isotope fractionation as it adsorbs onto mineral surfaces. Wasylenki et al. (2015) determined the $\Delta^{60}Ni_{ferrihydrite\text{-}fluid}$ during 25 ^{o}C adsorption experiments to be -0.35 ± 0.10‰. Similarly Gueguen et al. (2018) reported an identical $\Delta^{60}Ni_{ferrihydrite\text{-}fluid}$ = -0.35 ± 0.08‰. The adsorption of Ni from aqueous solution onto

goethite was reported to yield the greatest fractionation during Ni adsorption observed to date with $\Delta^{60}Ni_{goethite\text{-}fluid}$ = -0.77 ± 0.23‰ (Gueguen et al., 2018). Spivak-Birndorf et al. (2018) reported that nickel isotope fractionation from aqueous solution onto montmorillonite resulted in a $\Delta^{60}Ni_{montrormillinite\text{-}fluid}$ = -0.11 ± 0.09‰. These values are similar with those generated during the adsorption of Ni onto calcite in the present study, $\Delta^{60}Ni_{calcite\text{-}fluid}$ = -0.52±0.16‰ (2SD).

This study shows that calcite preferably adsorbs light Ni isotopes. In contrast, calcite preferentially adsorbs heavy Zn, with $\Delta^{66}Zn_{adsorbed\text{-}solution}$ averaging 0.41±0.18‰ and 0.73±0.08‰ in 0.1 and 0.7 M aqueous NaCl solutions, respectively (Dong and Wasylenki, 2016). The preferential uptake of heavy Zn was interpreted to stem from a change in coordination between the six-fold aqueous $Zn(H_2O)_6^{2+}$ complex and Zn adsorbed on the calcite surface, which has a four-fold coordination (Dong and Wasylenki, 2016). The tetrahedral coordination of Zn on the calcite surface was confirmed through EXAFS analysis (Elzinga and Reeder, 2002). Similarly changes in the coordination geometry of metal cations has shown has been shown to provoke substantial isotopic fractionation for the adsorption of Zn on the surfaces of quartz or amorphous SiO_2 (Nelson et al., 2017) and the adsorption of Ga isotopes on calcite and goethite surfaces (Yuan et al., 2018). This behavior of Zn fractionation during its adsorption to calcite contrasts with that of Ni, which likely does not change coordination number as it adsorbs to calcite surfaces from aqueous solution. In cases where coordination number does not change upon adsorption, small distortions of bond angles and lengths can also drive isotopic fractionation (Brennecka et al., 2011; Gueguen et al., 2018; Juillot et al., 2008; Wasylenki et al., 2015, 2014).

Several experimental and theoretical studies have been carried out to determine the Ni-O bond length in aqueous $Ni(H_2O)_6^{2+}$. Experimentally measured bond lengths range between 2.05-2.07 Å, as measured by XRD (Caminiti et al., 1977; Magini et al., 1982) and 2.07 Å, as measured by EXAFS (Sandstrom, 1979). These values are in good agreement with DFT (Density Functional Theory) calculations for the $Ni(H_2O)_{18}^{2+}$ cluster (2.073 Å, Fujii et al., 2011). They are slightly shorter than Ni-O bond length in gaspeite ($NiCO_3$) as determined by XRD (2.076 Å, Pertlik, 1986). These observations suggest that the adsorption of Ni from aqueous solution to calcite surfaces will result in a slight increase of the Ni-O bond length and induce an enrichment in light isotope of the adsorbed Ni surface complex.

Previous studies reported that the isotopic fractionation of metals between a fluid and a mineral phase also depends on the aqueous speciation of the metal (Balan et al., 2018; Fujii et al., 2011, 2014; Mavromatis et al., 2018; Schott et al., 2016). As our experiments were performed at pH ranging from 7.7 to 8.6, Ni aqueous speciation may have been impacted by the formation of $NiHCO_3^+$ and $NiCO_3°$ at the expense of aqueous Ni^{2+} with increasing pH. Based on the thermodynamic constants for the aqueous Ni species included in the minteq.v4 database, Ni^{2+} (referred to as $Ni(H_2O)_6^{2+}$ above) accounts for 92% of total dissolved Ni at pH 7.7 but for only 48% at pH 8.6. Aqueous Ni^{2+} is replaced by $NiHCO_3^+$ and $NiCO_3°$ as pH increases over this range in our solutions. Whereas the concentrations of $NiHCO_3^+$ and $NiCO_3°$ are negligible at pH 7.7, at pH 8.6 they represent 8 and 41% of dissolved nickel, respectively. Based on DFT calculations of reduced partition function ratios among Ni aqueous species reported by Fujii et al. (2014), the equilibrium fractionation factor at 25°C between aqueous Ni^{2+} and $NiCO_3°$ ($\Delta^{60}Ni_{Ni+2-NiCO3°}$) is equal to -0.402‰ and that between Ni^{2+} and $NiHCO_3^+$ ($\Delta^{60}Ni_{Ni+2-NiHCO3+}$) is -0.345‰. As such the nickel carbonate and bicarbonate complexes present in solution at pH 8.6 should make $Ni^{2+}_{(aq)}$ and adsorbed Ni ~0.2‰ lighter than at pH 7.7. The data of the present study do not, however, show enrichment of adsorbed Ni in light isotopes when the aqueous solution pH increases from 7.7 to 8.6; although there is some scatter apparent in Figure 6b, the data trend appears to show a slight increase in the uptake of heavier Ni with increasing pH. However, it should be noted that there is significant uncertainty in the calculated aqueous speciation of Ni as a function of pH in carbonate bearing solutions. For example, according to the stability constants values of aqueous $NiCO_3°$ and $NiHCO_3^+$ published by Baeyens et al. (2003), at pH 8.6 Ni^{2+} would account for 69% of the total dissolved Ni, and $NiCO_3°$ and $NiHCO_3^+$ for only 25 and 2%, respectively. The subsequent enrichment of $Ni^{2+}_{(aq)}$ and adsorbed Ni in light isotope would be of ~0.1‰, which is within the uncertainty our isotopic measurements – see Fig 6b.

4.3 Implications for natural systems.

A number of previous works have concluded that our current understanding of the Ni isotope balance in the oceans requires the identification of either another source of isotopically heavy Ni or another sink of isotopically light Ni. Various processes have been suggested as the possible light Ni sink including adsorption of Ni onto ferrihydrites or Mn-hydroxides and the incorporation of Ni into sedimentary sulfides (Gueguen et al., 2013; Vance et al., 2016;

Wasylenki et al., 2015). The present study considered the possibility that Ni adsorption onto calcite surfaces may also contribute to resolving this imbalance in the global marine Ni budget. This study shows that light Ni is preferentially adsorbed onto calcite as $\Delta^{60}Ni_{calcite\text{-}solution}$= -0.52±0.16‰. Although the mass of Ni removed from the ocean by adsorption onto calcite may be too small to resolve the currently perceived Ni isotope imbalance, considering the large mass of calcite formed annually, it may be a contributor to resolving this imbalance. The mass of Ni removed by its co-precipitation with calcite may however, be far more significant. A detailed calculation of such effects requires Ni fractionation factors during its co-precipitation, which will be explored in a future study.

5. CONCLUSIONS

Experiments in the present study were performed to determine the degree of Ni isotope fractionation imparted by the adsorption of Ni from an aqueous solution onto calcite surfaces. The major results include:

1) No variation of the isotopic composition of Ni adsorbed onto calcite was observed with time.

2) Calcite surfaces preferentially adsorb isotopically light Ni with an average $\Delta^{60}Ni_{calcite\text{-}fluid}$ = -0.52±0.16‰. This value is independent of the amount of adsorbed nickel, within uncertainty, indicating an equilibrium isotopic exchange process.

3) Ni does not change coordination number as it adsorbs to calcite surfaces from aqueous solution, however, the Ni-O interatomic distance is slightly longer for Ni adsorbed to calcite as it is for $Ni(H_2O)_6^{2+}$. This change in coordination geometry is likely the mechanism driving the fractionation of Ni isotopes during their incorporation on calcite.

ACKNOWLEDGEMENTS

The research was supported by ISONOSE a People Programme (Marie Curie Actions) of the European Unions' Seventh Framework Programme FP7/2017-2013/ under REA grant agreement n° [608069]. We thank Alain Castillo for BET measurements, Carole Causserand and Manuel Henry from the Géosciences Environement Toulouse for their assistance in the laboratories. We would also like to thank Giuseppe Saldi and Pascale Benezeth for helpful discussions.

REFERENCES

Atkins A. L., Shaw S., Peacock C. L., 2014. Nucleation and growth of todorokite from birnessite: Implications for trace-metal cycling in marine sediments. Geochim. Cosmochim. Acta. 144, 109-125.

Atkins, A.L., Shaw, S., Peacock, C. L., 2016. Release of Ni from birnessite during transformation of birnessite to todorokite: Implications for Ni cycling in marine sediments. Geochim. Cosmochim. Acta, 189, 158-183.

Baeyens, B., Bradbury, M.H., Hummel, W., 2003. Determination of aqueous nickel – Carbonate and nickel – Oxalate complexation constants. J. Solution Chem. 32, 319–339.

Balan, E., Noireaux, J., Mavromatis, V., Saldi, G.D., Montouillout, V., Blanchard, M., Pietrucci, F., Gervais, C., Rustad, J.R., Schott, J., Gaillardet, J., 2018. Theoretical isotopic fractionation between structural boron in carbonates and aqueous boric acid and borate ion. Geochim. Cosmochim. Acta 222, 117–129.

Balistrieri, L.S., Borrok, D.M., Wanty, R.B.,Ridley, W.I., 2008. Fractionation of Cu and Zn isotopes during adsorption onto amorphous Fe(III) oxyhydroxide: Experimental mixing of acid rock drainage and ambient river water. Geochim. Cosmochim. Acta 71, 311-328.

Barling, J., Anbar, A., 2004. Molybendum isotope fractionation durng adsorption by manganese oxides. Earth Planet. Sci. Let. 217, 315-329.

Belova, D. A., Lakshtanov, L.Z., Carneiro, J.F., Stipp, S.L.S., 2014. Nickel adsorption on chalk and calcite. J. Contam. Hydrol. 170, 1–9.

Brennecka, G.A., Wasylenki, L.E., Bargar, J.R., Weyer, S., Anbar, A.D., 2011. Uranium isotope fractionation during adsorption to Mn-oxyhydroxides. Environ. Sci. Technol. 45, 1370–1375.

Brunauer, S., Emmett, P.H., Teller, E., 1938. Adsorption of Gases in Multimolecular Layers. J. Am. Chem. Soc. 60, 309–319.

Cameron, V., Vance, D., 2014. Heavy nickel isotope compositions in rivers and the oceans. Geochim. Cosmochim. Acta 128, 195–211.

Cameron, V., Vance, D., Archer, C., House, C.H., 2009. A biomarker based on the stable isotopes of nickel Proc. Nat. Aca. Sci. 106, 10944–10948.

Chernonozhkin, S.M., Gideris, S., Lobo, L., Claeys, P., Vanhaecke, F., 2016. Development of an isolation procedure and MC-ICP-MS measurement protocol for the study of stable isotope

519 variations of nickel. J. Anal. Atomic Spectro. 30, 1518-1530.

520 Ciscato, E.R., Bontognali, T.R.R., Vance, D., 2018. Nickel and its isotopes in organic-rich
521 sediments: Implications for oceanic budgets and a potential record of ancient seawater. Earth
522 Planet. Sci. Let. 494, 239-250.

523 Criss, R.E., 1999. Principles of stable isotope distribution. Oxford University Press.

524 Dada, A.O., Adekola, F.A., Odebunmi, E.O., 2017. Kinetics, mechanism, isotherm and
525 thermodynamic studies of liquid phase adsorption of Pb^{2+} onto wood activated carbon
526 supported zerovalent iron (WAC-ZVI) nanocomposite. Cogent Chem. 3, 13516353.

527 Delstanche, S., Opfergelt, S., Cardinal,. D., Elass, F., Andre, L., Delcaux, B., 2009. Silicon
528 isotopic fractionation during adsorption of aqueous monosilic acid onto iron oxide.
529 Geochim. cosmochim. Acta 73, 923-934.

530 Dong, S., Wasylenki, L.E., 2016. Zinc isotope fractionation during adsorption to calcite at high
531 and low ionic strength. Chem. Geol. 447, 70–78.

532 Eiler, J.M., Bergquist, B., Bourg, I., Cartigny, P., Farquhar, J., Gagnon, A., Guo, W., Halevy, I.,
533 Hofmann, A., Larson, T.E., Levin, N., Schauble, E.A., Stolper, D., 2014. Frontiers of stable
534 isotope geoscience. Chem. Geol., 372, 119-143.

535 Elzinga, E.J., Reeder, R.J., 2002. X-ray absorption spectroscopy study of $Cu^{2+}$and Zn^{2+}adsorption
536 complexes at the calcite surface: Implications for site-specific metal incorporation
537 preferences during calcite crystal growth. Geochim. Cosmochim. Acta 66, 3943–3954.

538 Estrade, N., Cloquet, C., Echevarria, G., Sterckeman, T., Deng, T., Tang, Y.T., Morel, J.L., 2015.
539 Weathering and vegetation controls on nickel isotope fractionation in surface ultramafic
540 environments (Albania). Earth Planet. Sci. Let. 423, 24–35.

541 Fujii, T., Moynier, F., Blichert-Toft, J., Albarède, F., 2014. Density functional theory estimation
542 of isotope fractionation of Fe, Ni, Cu, and Zn among species relevant to geochemical and
543 biological environments. Geochim. Cosmochim. Acta 140, 553–576.

544 Fujii, T., Moynier, F., Dauphas, N., Abe, M., 2011. Theoretical and experimental investigation of
545 nickel isotopic fractionation in species relevant to modern and ancient oceans. Geochim.
546 Cosmochim. Acta 75, 469–482.

547 Gall, L., Williams, H.M., Siebert, C., Halliday, A.N., Herrington, R.J., Hein, J.R., 2013. Nickel
548 isotopic compositions of ferromanganese crusts and the constancy of deep ocean inputs and
549 continental weathering effects over the Cenozoic. Earth Planet. Sci. Let. 375, 148–155.

550 Gueguen, B., Rouxel, O., Ponzevera, E., Bekker, A., Fouquet, Y., 2013. Nickel Isotope
551 Variations in Terrestrial Silicate Rocks and Geological Reference Materials Measured by
552 MC-ICP-MS. Geostand. Geoanalytical Res. 37, 297–317.

553 Gueguen, B., Sorensen, J. V., Lalonde, S. V., Peña, J., Toner, B.M., Rouxel, O., 2018. Variable
554 Ni isotope fractionation between Fe-oxyhydroxides and implications for the use of Ni
555 isotopes as geochemical tracers. Chem. Geol. 481, 38–52.

556 Hoffmann, U., Stipp, S.L.S., 2001. The behavior of Ni^{2+} on calcite surfaces. Geochim.
557 Cosmochim. Acta 65, 4131–4139.

558 Jeandel, C., Oelkers, E.H., 2015. The influence of terrigenous particulate material dissolution on
559 ocean chemistry and global element cycles. Chem. Geol. 395, 50-66.

560 Juillot, F., Maréchal, C., Ponthieu, M., Cacaly, S., Morin, G., Benedetti, M., Hazemann, J.L.,
561 Proux, O., Guyot, F., 2008. Zn isotopic fractionation caused by sorption on goethite and 2-
562 Lines ferrihydrite. Geochim. Cosmochim. Acta 72, 4886–4900.

563 Lafuente, B., Downs, R.T., Yang, H., Stone, N., 2016. The power of databases: The RRUFF

564 Lakshtanov, L.Z., Stipp, S.L.S., 2007. Experimental study of nickel(II) interaction with calcite:
565 Adsorption and coprecipitation. Geochim. Cosmochim. Acta 71, 3686–3697.

566 Lemarchand, E., Schott, J., Gaillardet, J., 2005. Boron isotopic fractioantion related to boron
567 sorption on humic acid and th estructure of complexes formed. Geochim. Cosmochim. Acta
568 69, 3519-3533.

569 Lemarchand, E., Schott, J., Gaillardet, J., 2007. How surface complexes impact boron isotope
570 fractionation. Evidence from Fe and Mn oxides sorption experiments. Earth Planet. Sci. Let.
571 260, 277-296.

572 McBride, M.B., 1980. Chemisorption of Cd^{2+} on Calcite Surfaces. 1. Soil Sci. Soc. Am. J. 44, 26.

573 Nelson, J., Wasylenski, L., Cargar, J.R., Brown, G.E., Maher, K., 2017. Effects of surface
574 structural disorder and surface coverage on isotopic frationation during Zn (II) adsorption
575 onto quartz and amprphous silica surfaces. Geochim. Cosmochim. Acta 215, 354-376.

576 Oleze, M., von Blankenburg, F., Hoellen, D., Dietzel, M., Bouchez, J., 2014. Si stable isotope
577 fractionation during adsorption an the competition between kinetic and equilibrium isoopte
578 fractionation: Implications for weathering systems. Chem. Geol. 380, 161-171.

579 Parkhurst, D.L., Appelo, C.A.J., 2013. Description of input and examples for PHREEQC version
580 3 - A computer program for speciation, batch-reaction, one-dimensional transport, and
581 inverse geochemical calculations, in: U.S. Geological Survey Techniques and Methods,
582 Book 6, Chapter A43. U.S. Geological Survey, p. 497.

583 Peacock, C.L., Sherman, D.M., 2007. Sorption of Ni by birnessite: Equilibrium controls on Ni in
584 seawater. Chem. Geol. 238, 94–106. https://doi.org/10.1016/j.chemgeo.2006.10.019

585 Pokrovsky, O.S., Mielczarski, J.A., Barres, O., Schott, J., 2000. Surface Speciation Models of
586 Calcite and Dolomite/Aqueous Solution Interfaces and Their Spectroscopic Evaluation.

Langmuir 16, 2677–2688.

Pokrovsky, O.S., Schott, J., 2002. Surface chemistry and dissolution kinetics of divalent metal carbonates. Environ. Sci. Technol. 36, 426-432.

Pokrovsky, O.S., Schott, J., Thomas, F., 1999. Dolomite surface speciation and reactivity in aquatic systems. Geochim. Cosmochim. Acta 63, 3133–3143.

Pokrovsky , O.S., Galy, A., Schott, J., Pokrovski, G.S., Mantoura, S., 2014. Germanium, isotope fractionation during GE adsorption on goethite and its coprecipitation with Fe oxy (hydroxides). Geochim. cosmochim. Acta 131, 138-149.

Porter, S.J., Selby, D., Cameron, V., 2014. Characterising the nickel isotopic composition of organic-rich marine sediments. Chem. Geol. 387, 12–21.

Quitté, G., Oberli, F., 2006. Quantitative extraction and high precision isotope measurements of nickel by MC-ICPMS. J. Anal. At. Spectrom. 21, 1249–1255.

Reddy, M.M., Nancollas, G.H., 1971. The crystallization of calcium carbonate: I. Isotopic exchange and kinetics. J. Colloid Interface Sci. 36, 166–172.

Schott, J., Mavromatis, V., Fujii, T., Pearce, C.R., Oelkers, E.H., 2016. The control of carbonate mineral Mg isotope composition by aqueous speciation: Theoretical and experimental modeling. Chem. Geol. 445, 120-134.

Sclater, F.R., Boyle, E., Edmond, J.M., 1976. On the marine geochemistry of nickel. Earth Planet. Sci. Lett. 31, 119–128.

Sohrin, Y., Bruland, K.W., 2011. Global status of trace elements in the ocean. TrAC Trends Anal. Chem. 30, 1291–1307. https://doi.org/10.1016/J.TRAC.2011.03.006

Spivak-Birndorf, L.J., Wang, S.J., Bish, D.L., Wasylenki, L.E., 2018. Nickel isotope fractionation during continental weathering. Chem. Geol. 476, 316–326.

Stipp, S.L.S., Eggleston, C.M., Nielsen, B.S., 1994. Calcite surface structure observed at microtopographic and molecular scales with atomic force microscopy (AFM). Geochim. Cosmochim. Acta 58, 3023–3033.

Tahervand, S., Jalali, M., 2017. Sorption and desorption of potentially toxic metals (Cd, Cu, Ni and Zn) by soil amended with bentonite, calcite and zeolite as a function of pH. J. Geochemical Explor. 181, 1448-159.

Van Cappellen, P., Charlet, L., Stumm, W., Wersin, P., 1993. A surface complexation model of the carbonate mineral-aqueous solution interface. Geochim. Cosmochim. Acta 57, 3505–3518.

Vance, D., Little, S.H., Archer, C., Cameron, V., Andersen, M.B., Rijkenberg, M.J.A., Lyons,

T.W., 2016. The oceanic budgets of nickel and zinc isotopes: The importance of sulfdic environments as illustrated by the Black Sea. Philos. Trans. R. Soc. A Math. Phys. Eng. Sci. 374, 20150294. https://doi.org/10.1098/rsta.2015.0294

Wasylenki, L.E., Howe, H.D., Spivak-Birndorf, L.J., Bish, D.L., 2015. Ni isotope fractionation during sorption to ferrihydrite: Implications for Ni in banded iron formations. Chem. Geol. 400, 56–64.

Wasylenki, L.E., Swihart, J.W., Romaniello, S.J., 2014. Cadmium isotope fractionation during adsorption to Mn oxyhydroxide at low and high ionic strength. Geochim. Cosmochim. Acta 140, 212–226.

Yuan, W., Saldi, G.D., Chen, J., Vuccolini, M.V., Birck, J.-L., Liu, Y., Schott, J., 2018. Gallium isootpe fractionation during Ga adsorption on calcite and goethite. Geochim. Cosmochim. Acta 233, 350-363.

Zachara, J.M., Cowan, C.E., Resch, C.T., 1991. Sorption of divalent metals on calcite. Geochim. Cosmochim. Acta 55, 1549–1562.

Zachara, J.M., Kittrick, J.A., Harsh, J.B., 1988. The mechanism of Zn^{2+} adsorption on calcite. Geochim. Cosmochim. Acta 52, 2281–2291.